AD-A264 523 AGE

Form Approved
OME No. 0704-0188

1. AGENCY USE ONLY (Leave blank)	2. REPORT DATE 04/30/93	3. REPORT TYPE AND DATES COVERED Technical 06-01-92 to 05-31-93

4. TITLE AND SUBTITLE
Synthesis and Characterization of Mixed III-V and II-VI
Semiconductor Monomers Included in the Borate Sodalite
Analogue

5. FUNDING NUMBERS
N00014-90-J-1159

②

6. AUTHOR(S)
K.L. Moran, T.E. Gier, W.T.A. Harrison, G.D. Stucky,
and H. Eckert

7. PERFORMING ORGANIZATION NAME(S) AND ADDRESS(ES)
University of California
Department of Chemistry
Santa Barbara, CA 93106

8. PERFORMING ORGANIZATION REPORT NUMBER
T16

DTIC
ELECTE
MAY 18 1993
S
A
D

9. SPONSORING/MONITORING AGENCY NAME(S) AND ADDRESS(ES)
Office of Naval Research
Chemistry Program
800 N. Quincy Street
Alexandria, VA 22217

10. SPONSORING/MONITORING AGENCY REPORT NUMBER

11. SUPPLEMENTARY NOTES
Prepared for Publication in J. Am. Chem. Soc. (submitted)

12a. DISTRIBUTION/AVAILABILITY STATEMENT
Approved for public release;
distribution unlimited

12b. DISTRIBUTION CODE

13. ABSTRACT (Maximum 200 words)

The synthesis of the solid solution series $Ga_xZn_{(8-x)}[BO_2]_{12}P_xSe_{(2-x)}$ (x = 0, 0.5, 1, 2) is reported and the local and average long-range structures are discussed based on x-ray diffraction data, UV/visible spectroscopic measurements and a variety of field-dependent static and magic angle spinning and solid state NMR experiments. Inclusion of GaP within the borate sodalite analogue results in the formation of an isolated ^{31}P-$^{69,71}Ga$ dipolar spin pair that exhibits resolved J-coupling in the ^{31}P MAS NMR spectra. Theoretical analysis reveals that there are four different intracage structures distributed in small domains throughout the crystallographically single phase materials and these are identified as $[Zn_4Se]^{6+}$, $[GaZn_3P]^{6+}$, $[Zn_4P]^{5+}$ and, by inference, $[Ga_2Zn_2P]^{7+}$.

93 5 17 006

93-10935

14. SUBJECT TERMS	15. NUMBER OF PAGES 27
	16. PRICE CODE

17. SECURITY CLASSIFICATION OF REPORT Unclassified	18. SECURITY CLASSIFICATION OF THIS PAGE Unclassified	19. SECURITY CLASSIFICATION OF ABSTRACT Unclassified	20. LIMITATION OF ABSTRACT UL

Introduction

The optoelectronic properties of compounds can be dramatically altered by inclusion into the sodalite framework, which is one of several reasons why this zeolite structure type remains the focus of ongoing research efforts in many laboratories.[1] First described by Pauling in 1930,[2] the sodalite structure consists of a three-dimensional array of face-sharing cuboctahedral "cages" supported by intracage tetrahedra, a schematic of which is shown in Figure 1. The general composition of the cubic sodalite unit cell is $M_8X_2[TO_2]_{12}$, in which tetrahedral atoms, T, linked by bridging oxygens[3] form the framework that encloses charge-balancing M_4X tetrahedra. Both naturally-occurring and synthetic isotypes are known for a myriad of compositions[4] (M = Li, Na, K, Ag, Ca, Sr, Zn, Cd, . . .; X = Br, Cl, OH, O, S, Se, Te, SO_4, WO_4, . . .; T = Be, B, Al, Ga, Si, Ge, . . .).

Sodalite oxide frameworks typically have high dielectric constants[5] and act as electrostatic barriers between adjacent cages, an isolation effect that perturbs the electronic structure of the intracage species. Inclusion of potassium halide into aluminosilicate sodalite, for example, results in enhanced cathodochromic sensitivity and these materials are used in display devices.[6] This enhancement due to inclusion has been attributed to framework-assisted isolation of individual F centers, electrons trapped at halogen vacancies, as well as greater separation of the electrons from the hole centers with which they recombine.

The framework electrostatic isolation effect is observed readily by MAS NMR spectroscopy of the cage center anions. The single ^{77}Se MAS NMR resonance of the sodalite analogue zinc selenide borate, $Zn_8Se_2[BO_2]_{12}$, is shifted far upfield relative to bulk $ZnSe^7$ which suggests greater localization of electron density at the cage center; that is, the delocalization of the bulk semiconductor is blocked by the framework electric field and by the extended cage-to-cage distance. Cage size and separation distance can be controlled by substitution of the framework atoms with consequent changes in the optoelectronic properties, as demonstrated in the genthelvites.[8]

Another method for fine-tuning the optoelectronic properties of sodalites is to vary the intracage composition. For example, deposition of sodium vapor onto the optically transparent sodalite $Na_6[AlSiO_4]_6^9$ results in the buildup of $Na_4^{4+}[e^-]$ clusters inside the cages, in which the electron, e^-, is not tightly bound to the cluster.[10] By controlling the amount of sodium that enters the cages, materials which range in color from pale blue to black are synthesized.[11]

As part of ongoing investigations of the correlations between structure, composition and optoelectronic properties in sodalite materials, we report the synthesis and characterization of the solid solution series $Ga_xZn_{(8-x)}P_xSe_{(2-x)}[BO_2]_{12}$. The borate sodalite framework has a net charge of -6 which is compensated by a $[Zn_4Se]^{6+}$ tetrahedron inside each cage. Substitution of isovalent GaP for ZnSe is possible due to the size similarities of the ions; the covalent radii of Ga, Zn, P and Se are 1.26, 1.25, 1.06 and 1.16 Å, respectively. We describe the average long-range structure of these materials based on results of powder x-ray diffraction and UV/Visible spectroscopic measurements. Local electronic effects and compositional variations are characterized by MAS NMR spectroscopy, a technique well known for elucidation of short range order in amorphous materials.[12] We report the ^{77}Se MAS NMR spectra of the cage center anions and a detailed analysis of the ^{31}P MAS NMR spectra of the GaP-substituted species measured at different magnetic field strengths.

Experimental Section

Materials. Boric acid and zinc oxide, ZnSe and GaP were used as purchased from Fisher Scientific and Strem Chemicals, Inc., respectively.

Synthesis. A starting material of stoichiometry ZnB_2O_4 was prepared from ZnO and boric acid heated in air at 550 °C for several hours; powder XRD showed this to be a mixture of ZnB_4O_7 and ZnO. This material was ground well with a stoichiometric amount of the III-V or II-VI compound, loaded into a graphitized quartz ampule,[13] heated gently under vacuum with a torch to remove physisorbed water and flame-sealed. The sealed ampules were heated in a furnace at 900 to 950 °C for 12 to 36 hours. The products, recovered as powders, generally contain excess bulk semiconductor. All of the bulk GaP and most of the ZnSe were removed by stirring the powders for 48 hours in an aqueous solution of Br_2 adjusted to a pH of 6 with hypochlorite solution (bleach). Previously we reported[7] the optical spectrum of $Zn_8Se_2[BO_2]_{12}$, which we had mistakenly believed was free of bulk ZnSe; subsequent experiments have revealed that the absorption at 475 nm, erroneously attributed to the sodalite, is due to residual bulk ZnSe in the sample.

Characterization. Powder x-ray diffraction data were collected on a Scintag Pad-X theta-theta diffractometer using Cu Kα radiation with Si as an internal standard. Rietveld structural refinement of the solution end members was performed with the program GSAS[14] using $Zn_8O_2[BO_2]_{12}$ as a starting model.[15] The structure of $Zn_6Ga_2P_2[BO_2]_{12}$ was refined by constraining Zn and Ga as equivalent atoms. Elemental analysis, performed

at Galbraith Laboratories, Knoxville, TN, on a sample with x = 1, reveals a Ga/P ratio of unity as expected.

UV/Visible spectra were obtained in reflectance mode using a $BaSO_4$ integrating sphere on a Cary-14 monochromator upgraded with a computer interface by On-Line Instrument Systems, Inc., Bogart, GA. Spectra were corrected against a $BaSO_4$ background.

All of the NMR experiments were performed on a General Electric GN-300 spectrometer using 7.0 and 4.7 T magnets, and using high speed MAS probes manufactured by Doty Scientific, Inc., Columbia, SC. ^{77}Se MAS NMR data were collected at a spectral frequency of 57.3 MHz (7.0 T) using a pulse width of 8.5 μs and recycle delay of at least 30 minutes; chemical shifts are referenced to CdSe. Measurement of the ^{71}Ga MAS NMR signal was attempted at both 7.0 and 4.7 T field strengths (93 and 61 MHz, respectively) with a 2 μs pulse width and 1 second delay. ^{31}P MAS NMR spectra were measured at frequencies of 121.6 (7.0 T) and 81.0 (4.7 T) MHz. A pulse width of 2.25 μs was used with a recycle delay of 10 min and spectra are referenced to H_3PO_4. Static ^{31}P spin echo measurements were made at 7.0 T using a $\pi/2$-t_1-π pulse sequence, with the 90° pulse width set to 6.25 μs. ^{31}P MAS spectral spin diffusion experiments were performed at 4.7 T using a rotor-synchronized DANTE pulse sequence $(\theta - t_r^{-1})_n$-τ-$\pi/2$.[16] One signal was set on resonance at approximately 81 MHz and selectively inverted by a total of ten short pulses of width 1.25 μs separated by 150 μs. Four scans were acquired at a total of seven different τ delays, ranging from 50 ms to 900 s, with a recycle delay of 15 minutes.

Results and Discussion

The compounds in the $Ga_xZn_{(8-x)}P_xSe_{(2-x)}[BO_2]_{12}$ series crystallize in the body-centered cubic space group I43m. Unit cell parameters, which follow Vegard's Law for the solution series, and selected distances are listed in Table I. Because the electron densities of zinc and gallium are nearly identical (atomic numbers 30 and 31, respectively) it is not possible to distinguish between these two atoms by x-ray diffraction techniques when they occupy the same crystallographic site: the reported distances are mean values for the four cations inside the cage. Atomic coordinates, thermal parameters and an ORTEP diagram of the structure are submitted as supplementary material.

The results of UV/Vis spectroscopic measurements, shown in Figure 2. describe the average electronic structure of these inclusion materials. The absorption bands of the GaP-containing solutions indicate the existence of a well-defined direct electronic transition in the sodalites. In the ZnSe end member (x = 0) the absorption edge is presumably deep in the

UV region and beyond the measurement capabilities of our instrumentation; blue-shifted significantly relative to bulk ZnSe which absorbs at 480 nm. The spectrum of the end member $Zn_6Ga_2P_2[BO_2]_{12}$ is blue-shifted relative to bulk GaP (554 nm) and exemplifies the electronic isolation effect as a result of inclusion. The two solid solutions (x = 0.5 and x = 1) exhibit identical electronic transition energies, within experimental error, that are apparently intermediate between those of the two end members. This observation suggests that in the GaP end member, for example, there may exist weak cage-to-cage electronic coupling that is interrupted as ZnSe is introduced into the framework. None of the samples exhibited room temperature luminescence; the nonradiative relaxation implies strong coupling to lattice phonons.

Evidence of the electrostatic isolation effect of the framework is provided by MAS NMR of the central anions in the series. Within experimental error, the ^{77}Se MAS spectra are invariant to substitution with GaP in the structure. Each solid solution (x = 0, 0.5, 1) has a single ^{77}Se resonance at approximately -327 ppm relative to CdSe. The fact that the shift does not change as GaP is added to the structure indicates that the cage center is electronically isolated from neighboring cages. Following the usual chemical shift arguments, the upfield chemical shift relative to that of bulk ZnSe, at +124 ppm, reflects a diminished paramagnetic contribution, suggesting a greater localization of electron density at the cage center.

Analogous to the ^{77}Se MAS results, the ^{31}P MAS NMR spectra are invariant to substitution in the series $Ga_xZn_{(8-x)}P_xSe_{(2-x)}[BO_2]_{12}$, as shown in Figure 3, and the resonances are shifted upfield compared with that of bulk GaP (-143 ppm relative to H_3PO_4). Unlike the ^{77}Se MAS NMR spectra, however, the ^{31}P MAS NMR spectra consist of two groups of peaks: a multiplet of three peaks with the intensity ratio 1:1:2, the center of gravity of which is positioned at -398 ppm, and a single peak at -453 ppm. The ^{31}P MAS spectra of $Ga_2Zn_6P_2[BO_2]_{12}$ at two magnetic field strengths, 4.7 and 7.0 T, are shown in Figure 4 and the chemical shifts and peak separations within the multiplet A-C and the single peak D are listed in Table II.

As revealed by Figure 4 and Table II, the peak positions of A-C on a ppm scale are field dependent and hence are ascribed to $^{69,71}Ga,^{31}P$ indirect spin coupling. Since ^{69}Ga (natural abundance 60.4%) and ^{71}Ga (39.6%) both have a nuclear spin of 3/2, one might anticipate the high resolution ^{31}P MAS NMR spectrum of a molecule containing the $^{69,71}Ga,^{31}P$ spin pairs to consist of four equally-spaced peaks, each associated with one of the allowed components of $^{69,71}Ga$ nuclear spin along the magnetic field, m_s. However, the asymmetric and field dependent separations within the multiplet at -398 ppm (Figure 4) indicate a strong perturbation of the $^{69,71}Ga$ Zeeman levels by the quadrupolar interaction.

One consequence of the so-called breakdown of the high-field approximation is that dipolar interactions involving quadrupolar nuclei are not completely eliminated by magic angle spinning.[18] As a result, high-resolution MAS NMR spectra of spin-1/2 nuclei that are J-coupled to quadrupolar nuclei are not generally symmetrical. Instead, the separations between the peaks are "squeezed" at one end and "stretched" at the other.[19-25]

In cases where the quadrupolar coupling constant, χ, is smaller than the Zeeman interaction, such quadrupolar perturbed multiplets in the MAS NMR spectra of spin-1/2 nuclei have been successfully analyzed by application of first order perturbation theory.[18] To first order, the ^{31}P MAS NMR transitions of phosphorus indirect and direct spin-spin coupling with a quadrupolar nucleus S are given by:[26]

$$\nu_m = -m \, |J| - \frac{S(S+1) - 3\,m^2}{S(2S-1)} \, d \qquad (1)$$

where J is the $^{69,71}Ga,^{31}P$ indirect spin-spin coupling constant, S = 3/2 for $^{69,71}Ga$, m = 3/2, 1/2, -1/2, and -3/2, and the residual dipolar coupling d is given by:

$$d = \frac{3\chi(D - \Delta J/3)}{20\nu_s} \, [3\cos^2\beta^D - 1 + \eta\sin2\beta^D\cos^2\alpha^D] \qquad (2)$$

D is the Ga,P direct dipolar coupling constant, dependent on the inverse cube internuclear separation, ΔJ is the anisotropy in the indirect spin-spin coupling tensor, ν_s is the ^{69}Ga or ^{71}Ga Larmor frequency (48.14 and 61.16 MHz at B_0 = 4.7 T), χ is the ^{69}Ga or ^{71}Ga nuclear quadrupolar coupling constant, $e^2q_{zz}Q/h$, and η is a parameter which describes the asymmetry of the electric field gradient (EFG) tensor at the Ga nucleus, $(eq_{xx} - eq_{yy})/eq_{zz}$, with $|eq_{zz}| \geq |eq_{yy}| \geq |eq_{xx}|$. The azimuthal and polar angles α^D and β^D define the orientation of the dipolar vector in the principal axis system of the EFG tensor. In Equation 2 we have assumed that the unique component of the J-tensor is parallel to the dipolar vector. To first order, the appearance of the spectrum is independent of the sign of J.[18]

From the two ^{31}P MAS NMR spectra obtained at different magnetic field strengths, the multiplet centered at -398 ppm can be analyzed unambiguously to yield values of the indirect spin-spin coupling constants, J, and the residual dipolar coupling, d. In order to obtain calculated spectra shown in Figure 4, both isotopes ^{69}Ga and ^{71}Ga were included into the calculation with J and d scaled according to the magnetogyric ratios, $\gamma(^{69}Ga)/\gamma(^{71}Ga) = 0.787$, and nuclear quadrupole moments, $Q(^{69}Ga)/Q(^{71}Ga) = 1.59$. respectively.[27,28] Although the presence of the minor component $^{71}Ga,^{31}P$ does not result in additional peaks within the multiplets shown in Figure 4, it causes shoulders most

apparent in the low frequency region of the ^{31}P MAS NMR spectrum obtained at 81 MHz. The parameters used to generate the calculated spectra shown in Figure 4 are: $J(^{69}Ga,^{31}P)$ = 560 Hz, $J(^{71}Ga,^{31}P)$ = 712 Hz, and $d(^{69}Ga)$ = +192 Hz, $d(^{71}Ga)$ = +121 Hz at 4.7 T and $d(^{69}Ga)$ = +128 Hz, $d(^{71}Ga)$ = +81 Hz at 7.0 T. A mixed Gaussian-Lorentzian line broadening function consisting of 75% Gaussian line shape and line widths of 400 Hz (4.7 T) and 600 Hz (7.0 T) were employed. Since the ratio of the line widths observed at the two different magnetic field strengths are proportional to the strength of B_0, a chemical shift dispersion appears to be the source of these rather broad peaks.

The observation of spin-spin coupling of phosphorus to one gallium nucleus is attributed to a $[GaZn_3P]^{6+}$ cage, in which gallium is tetrahedrally coordinated to one phosphorus and three oxygens. Based on this three-fold local symmetry at the site of the gallium nucleus, the $^{69,71}Ga,^{31}P$ dipolar vector is assumed to be collinear (β^D = 0) with the z-axis of the axially symmetric EFG tensor (η = 0). Assuming crystallographic site equivalence of the Ga and Zn atoms in the structure, the calculated Ga-P separation is 2.207 Å, from which the dipolar coupling constants for the spin pairs $^{69}Ga,^{31}P$ (1060 Hz) and $^{71}Ga,^{31}P$ (1350 Hz) can be calculated. Furthermore, if $\Delta J/3$ is assumed to be negligible, it is possible to use Equation 2 to estimate the quadrupolar coupling constants for the gallium atoms to be -29 MHz (^{69}Ga) and -18 MHz (^{71}Ga). While these are only crude estimates, it is clear that the Ga quadrupolar coupling constants are of the same order of magnitude as the Larmor frequencies at 4.7 T. Consequently, large second-order quadrupolar broadening in excess of 200 kHz is anticipated and probably explains our inability to detect a ^{71}Ga NMR signal.

The peak at -453 ppm in the ^{31}P MAS NMR spectrum must be attributed to a different type of phosphorus species not bonded to gallium. The question remains as to the nature of the nearest neighbor environment of the phosphorus nucleus. The relative spin counts of the ^{31}P resonances indicate that this singlet moiety accounts for 12 to 14% of the total phosphorus in each sample; if this represents a separate crystallographic phase it would be detected by high resolution XRD measurements, unless, of course, the symmetry and the lattice parameters are equivalent to the solution containing the Ga-coupled phosphorus.

To address the question of possible phase separation in these samples, ^{31}P MAS spectral spin diffusion measurements were carried out between the dominant signal near -403 ppm and the peak at -453 ppm. As previously shown, spectral spin diffusion is a sensitive probe of the dipole-dipole interactions between two spins which are close enough spatially to exchange Zeeman polarization. Such exchange is possible even for inequivalent sites because there is level crossing during the MAS rotor period.[29] The rate of spin

diffusion decreases as the spatial separation increases, proportional to the inverse sixth power of the internuclear distance.[30] Thus we would expect no net polarization transfer in our materials if they were phase separated.

The results of the spin diffusion experiment for the $Ga_2Zn_6P_2[BO_2]_{12}$ sample are shown in Figure 5. In this case the strongest resonance at -403 ppm has been selectively inverted with the DANTE sequence and the system is allowed to relax for a time τ before application of a nonselective $\pi/2$ pulse prior to the FID acquisition. Measurements are made at varying τ and the resulting spectra are a map of the time-dependent polarization transfer between spins at different frequencies. The detailed τ-dependence of the normalized resonance intensity for the -453 ppm peak is given in the figure caption. The apparent initial slight increase at very short τ values is most likely due to imperfections in the DANTE sequence. The subsequent decrease over the time interval $2 \text{ s} \leq \tau \leq 60 \text{ s}$ is evidence of spin diffusion. At longer τ values, the peak intensities increase again due to the effects of spin-lattice relaxation. While magnetization transfer is most efficient within the J-coupled multiplet, as expected, the decrease observed in the intensity of the singlet at -453 ppm clearly indicates spatial proximity between the two types of phosphorus atoms. Likewise, selective inversion of the ^{31}P resonance at -453 ppm shows cross-relaxation effects involving the J-coupled multiplet. The distance between P nuclei in adjacent cages in this sample is 6.594 Å, which is of appreciable magnitude and explains the overall weakness of the effect. Based on these results and the XRD observations, it is reasonable to assume that the material is single phase and that the two types of phosphorus reside in adjacent cages.

For a satisfactory explanation of the bonding environment of the upfield singlet phosphorus species, we turn to the information provided by the chemical shift. In keeping with our previous arguments, the fact that the chemical shift of the singlet is upfield relative to the Ga-coupled phosphorus suggests that there is greater electron density at the singlet site, and based on the absence of spinning sidebands and observable J-coupling, evident from the ^{31}P MAS NMR spectrum at 7.0 T shown in Figure 4, a rather symmetrical environment is expected for this species. This electronic environment can be attained by substituting the more electropositive nucleus zinc in place of the gallium. Therefore we assign the signal at -453 ppm to a phosphorus coordinated to four zinc atoms, which forms the tetrahedron $[Zn_4P]^{5+}$.

Stoichiometrically there is one Ga for every P nucleus in the material, as confirmed by elemental analysis, which must be accounted for in the model we describe. Based on the spin diffusion results, and consideration of stoichiometric and charge restrictions, the $[Zn_4P]^{5+}$ cage center is most likely adjacent to a cage containing $[Ga_2Zn_2P]^-$. While we

do not observe a corresponding ^{31}P signal for such a species, we expect the signal intensity to be spread out even farther due to the stronger ^{69,71}Ga,^{31}P dipole coupling and the increased J-coupling multiplicity. Possibly the ^{31}P signal for this species is either broadened beyond detection or obscured by the spectrum attributed to the $[GaZn_3P]^{6+}$ species. Unfortunately there are no known model compounds containing Zn and Ga in the nearest neighbor environment of a tetrahedrally coordinated P atom; therefore it is not possible to provide more definitive evidence of this assignment.

While charge restrictions require proximity of the $[Zn_4P]^{5+}$ and $[Ga_2Zn_2P]^{7+}$ cages, the overall distribution of the four intracage species throughout the structure remains to be addressed. The lack of any significant trend of ^{31}P and ^{77}Se chemical shifts with composition argues in favor of P-rich and Se-rich micro-domains. More precise information about this distribution is obtained by measuring the homonuclear dipole-dipole couplings between the phosphorus cage centers. The internuclear distances between like nuclei in a solid are related to the second moment, M_{2d}, of the NMR spectral resonance line by the following equations, derived from van Vleck theory:[31]

$$M_{2d} = 3/5 \ (\mu_0 / 4\pi)^2 \ I(I+1) \ \gamma^4 \hbar^2 \ N^{-1} \sum_{i \neq j} d_{ij}^{-6} \qquad (3a)$$

or

$$M_{2d} = 4/15 \ (\mu_0 / 4\pi)^2 \ I(I+1) \ \gamma^4 \hbar^2 \ N^{-1} \sum_{i \neq j} d_{ij}^{-6} \qquad (3b)$$

where γ is the gyromagnetic ratio, I is the spin quantum number and N is the number of nuclei for which M_{2d} is calculated. Equation 3a is used if the interacting nuclei have identical resonance frequencies. On the other hand, if the interacting nuclei have resonance frequency differences that are large compared to the dipolar coupling constant, Equation 3b must be used. The latter is often the case if inhomogeneous broadening, site distribution effects or heteronuclear dipolar couplings create magnetic inequivalences. As discussed above, there are strong static heteronuclear ^{69,71}Ga,^{31}P interactions in these materials; we would expect that the measured values of M_{2d} would approximate those given by Equation 3b.

Experimentally, the second moment is measured by the pulse sequence $\pi/2$-t_1-π. The static spin echo technique serves to refocus all interactions linear in I_z resulting in the formation of an echo of the signal at time $2t_1$.[32] The homonuclear spin-spin interactions are not refocussed in this experiment and thus cause a decay in the intensity of the spin echo with increasing evolution time $2t_1$. Assuming multiple spin interactions, the decay is approximated as Gaussian and is given by:

$$I(2t_1)/I(0) = \exp\{-M_{2d}(2t_1)^2/2\} \qquad (4)$$

where $I(0)$ is the extrapolated intensity of the echo at the time origin. Previous studies of model compounds have shown that this analysis yields the correct M_{2d} values as predicted from Equation 3b.[33]

The spin echo decay and the fit to Equation 4 for the solid solution $x = 1$ are shown in Figure 6, from which it is clear that the Gaussian approximation is valid for these materials. Figure 7 compares the measured and calculated second moments for all of the samples studied. The curves at a and c, from Equations 3a and 3b respectively, are calculated assuming all cage centers are occupied by phosphorus; thus only the cage-to-cage distance, based on unit cell size, affects the magnitude of M_{2d}. These curves describe the results expected if the samples formed P- and Se-rich micro-domains. On the other hand, the dashed lines b and d correspond to M_{2d} calculated for a completely random distribution of P- and Se-filled cages in the samples, based on Equations 3a and 3b, respectively, and account for the increasing P-P distances (on average) as ZnSe is added to the structure. All of the calculated curves include homonuclear dipolar interactions from the first, second, and third nearest neighbor spheres, with a total radius of about 20 Å.

The measured second moments of the solid solutions most closely resemble curve c, which indicates that there is much stronger homonuclear dipolar coupling than would be expected based on a random distribution of phosphorus in the solutions. These data are evidence of phosphorus-rich domains in the solutions and the moderate decrease in M_{2d} with decreasing phosphorus concentration suggests that the domains are so small in size that they possess a considerable percentage of P atoms on their "surfaces."

The calculated curves in Figure 7 do not account for the coupled $[Zn_4P]^{5+}$ and $[Ga_2Zn_2P]^{7+}$ cages. It is reasonable to assume that these cages would be joined at the 6-ring faces of the cuboctahedra, which represent the smallest distance between the contents of adjacent cages. Preferential contact through the 6-ring faces would result in stronger ^{31}P-^{31}P homonuclear dipolar coupling and hence a larger M_{2d} than that calculated for curve c. Because the samples exhibit strong heteronuclear dipolar coupling, which discounts the use of Equation 1a (curves a and b) for these solutions, we believe that the discernible discrepancy between the observed and calculated M_{2d} may be attributable to these preferential cage contacts.

Summary

Inclusion of ZnSe and GaP in the borate sodalite framework results in intriguing local and average long-range optoelectronic properties. The materials are single phase solutions that exhibit interesting optical absorption features. The absorption edge of ZnSe borate is apparently blue-shifted, relative to bulk ZnSe, to the far UV region and that of the GaP-included end member is blue-shifted significantly from bulk GaP. The average optoelectronic properties of the two solutions are identical and the common absorption edge appears at an energy somewhere between the two end members. These results suggest that there is a cooperative electronic effect between like cages in the pure end members that is blocked in the solutions as the contents vary from cage to cage.

MAS NMR chemical shift measurements suggest that the sodalite structure serves to isolate, electronically and magnetically, the species within the cages. In the GaP-included sodalite, a special case of an isolated $^{69,71}Ga, ^{31}P$ dipolar spin pair is observed and the J-coupling in this material has been theoretically modelled and discussed. Four different intracage structures have been identified in these single phase materials as $[Zn_4Se]^{6-}$, $[GaZn_3P]^{6+}$, $[Zn_4P]^{5+}$ and, by inference, $[Ga_2Zn_2P]^{7+}$. Measurement of the homonuclear $^{31}P-^{31}P$ dipolar coupling strength indicates that the phosphorus-containing cages are not distributed randomly throughout the sodalite structure; rather they group together in micro-domains. These domains, however, are too small to be detected by lab source x-ray diffraction.

Identification of the intracage compositions cannot be confirmed by x-ray diffraction due to the similarity in electron density between the zinc and gallium atoms; with neutron diffraction data it may be possible to confirm the existence of these moieties and to observe the small domains. Overall, the results of this study illustrate the power of combined selective ^{31}P NMR approaches to elucidate the local electronic structures and atomic arrangements present in these nanocomposites.

References

1. See, for example: Stucky, G. D.; Srdanov, V. I.; Harrison, W. T. A.; Gier, T. E.; Keder, N. L.; Moran, K. L.; Haug, K.; Metiu, H. I.; in "Supramolecular Architecture: Synthetic Control in Thin Films and Solids"; Bein, T., Ed.; American Chemical Society: Washington, D. C., 1992; 294-313. Ozin, G. A.; Kuperman, A.; Stein, A. Angew. Chem. Int. Ed. Engl. 1989, 28, 359-376.

2. Pauling, L. Z. Krist. 1930, 74, 213-225.

3. The synthesis of a nonoxide-framework sodalite analogue has been reported by Schnick, W.; Lucke, J. Angew. Chem. Int. Ed. Engl. 1992, 31, 213-215.

4. Taylor, D. Contr. Mineral. and Petrol. 1967, 16, 172-188.

5. Van Doorn, C. Z.; Schipper, D. J.; Bolwijn, P. T.; J. Electrochem. Soc. 1972, 119, 85.

6. Faughnan, B. W.; Heyman P. M.; Gorog, I.; Shidlovsky, I. Advances in Image Pickup and Display, Volume 4; Academic Press, Inc.: 1981, 87-155.

7. Moran, K. L.; Ott, A. W.; Gier, T. E.; Harrison, W. T. A.; Eckert, H.; Stucky, G. D. Mat. Res. Soc. Symp. Proc. 1992, 242, 249-254.

8. Moran, K. L.; Gier, T. E.; Ott, A. W.; Harrison, W. T. A.; Eckert, H.; Stucky, G. D. (manuscript in preparation).

9. $Na_6[AlSiO_4]_6$ is the dehydroxylated and dehydrated form of $Na_8[AlSiO_4]_6(OH)_2 \cdot 2H_2O$. See, for example, Engelhardt, G.; Felsche, J.; Sieger, P. J. Am. Chem. Soc. 1992, 114, 1173-1182.

10. Haug, K.; Srdanov, V. I.; Stucky, G. D.; Metiu, H. J. Chem. Phys 1992, 96, 3495.

11. Srdanov, V. I.; Haug. K.; Metiu, H.; Stucky, G. D. J. Phys. Chem. 1992, 96, 9039-9043.

12. Eckert, H. Prog. NMR Spectrosc. 1992, 24, 159-293.

13. To prevent reaction of borate starting materials with the quartz, ampules were coated with graphite: the inside walls of the ampule are wetted with acetone and strongly heated with a torch until completely coated.

14. Larson, A. C.; Von Dreele, R. B. GSAS Users Guide. Los Alamos Report. 1988, LAUR 86-748.

15. Smith-Verdier, P.; Garcia-Blanco, S. Z. Krist. 1980, 151, 175.

16. Caravatti, P.; Levitt, M. H.; Ernst, R. R. J. Magn. Reson. 1986, 68, 323

17. Donnay, J. D. H.; Ed. "Crystal Data: Determinative Tables", 3rd Ed. Vol. 4, 1978: JCPDS-International Centre for Diffraction Data, Swarthmore, PA.

18. Harris, R. K.; Olivieri, A. C. Progr. NMR Spectroscr. 1992, 24, 435-456.

19. Menger, E. M.; Veeman, W. S. J. Magn. Reson. 1982, 46, 257.

20. Harris, R. K.; J. Magn. Reson. 1988, 78, 389.

21. Olivieri, A. J. Am. Chem. Soc. 1992, 114, 5758.

22. Chu, P.-J.; Lunsford, J. H.; Zalewski, D. J. J. Magn. Reson. 1990, 87, 68.

23. Lindner, E.; Fawzi, R.; Mayer, H. A.; Eichele, K.; Pohmer, K. Inorg. Chem. 1991, 30, 1102.

24. Gobetto, R.; Harris, R. K.; Apperley, D. C. J. Magn. Reson. 1992, 96, 119.

25. Eichele, K.; Wasylishen, R. E.; Corrigan, J. F.; Doherty, S.; Sun, Y.; Carty, A. J. Inorg. Chem. 1993, 32, 121.

26. Olivieri, A. C. J. Magn. Reson. 1989, 81, 201.

27. Mason, J., Ed. "Multinuclear NMR", Plenum Press: New York, 1987.

28. Popkova, L. A.; Guryanova, E. N.; Volkov, A. F. J. Mol. Struct. 1982, 83, 341.

29. Zhang, Z.; Kennedy, J. H.; Eckert, H. J. Am. Chem. Soc. 1992, 114, 5775- Moran, L. B.; Berkowitz, J. K.; Yesinowski, J. P. Phys. Rev. B 1992, 45, 5347.

30. Kubo, A.; McDowell, C. A. J. Chem. Soc. Faraday Trans. 1. 1988, 84, 3713-3730. Suter, D.; Ernst, R. R. Phys. Rev. B. 1985, 32, 5608-5627.

31. Van Vleck, J. H. Phys. Rev. 1948, 74, 1168.

32. Lathrop, D.; Eckert, H. J. Amer. Chem. Soc. 1989, 111, 3536-3541.

33. Franke, D. R.; Maxwell, R. S.; Lathrop, D.; Eckert, H. J. Am. Chem. Soc. 1991, 113, 4822- Lathrop, D.; Franke, D. R.; Maxwell, R. S.; Tepe, T.; Flesher, R.; Zhang, Z.; Eckert, H. Solid State Nucl. Magn. Reson. 1992, 1,

Table II. Chemical Shifts in ppm (vs. H_3PO_4) and Peak Separations in Hz of the ^{31}P Resonances in $Ga_xZn_{(8-x)}P_xSe_{(2-x)}[BO_2]_{12}$.

$\underline{B_0 = 7.0\ Tesla}$

comp.	A	B	C	D	A-B	B-C	A-C
x = 2	-390.0	-396.9	-402.0	-453.6	838	697	1535
x = 1	-389.4	-396.3	-401.5	-453.1	843	628	1471
x = 0.5	-388.8	-395.1	-400.3	-453.0	809	628	1437

$\underline{B_0 = 4.7\ Tesla}$

comp.	A	B	C	D	A-B	B-C	A-C
x = 2	-384.8	-396.2	-403.9	-453.0	922	628	1550
x = 1	-384.3	-395.3	-403.9	-453.0	889	698	1587
x = 0.5	-383.9	-394.5	-402.2	-452.1	858	628	1486

Figure Captions

Figure 1. A schematic diagram of the sodalite structure with composition $M_8X_2[TO_2]_{12}$. The T atoms are represented by vertices of the cuboctahedral cages and are connected via bridging oxygens which are not shown. The central anion X is represented by the large circle at the centers of the cages, surrounded by four M atoms in a tetrahedral arrangement; the cations point toward the 6-ring faces.

Figure 2. UV/Vis Reflectance spectra for the solid solutions $Ga_xZn_{(8-x)}P_xSe_{(2-x)}[BO_2]_{12}$ (a) x = 2; (b) x = 1; (c) x = 0.5.

Figure 3. ^{31}P MAS NMR spectra for the series $Ga_xZn_{(8-x)}P_xSe_{(2-x)}[BO_2]_{12}$ measured at a magnetic field strength of 4.7 Tesla. (a) x = 2; (b) x = 1; (c) x = 0.5.

Figure 4. Field dependent ^{31}P MAS spectra of $Ga_2Zn_6P_2[BO_2]_{12}$. Experimental spectra at (a) 4.7 T and (b) 7.0 T. Spinning sidebands are labelled with asterisks and chemical shifts of signals A, B, C and D are listed in Table II. Computer simulated spectra at (c) 4.7 T and (d) 7.0 T, using the parameters described in the text.

Figure 5. Results of the ^{31}P spin diffusion experiment for the $Ga_2Zn_6P_2[BO_2]_{12}$ sample. The intensity of the signal at -453 ppm changes in the following manner:

τ	$I(\tau)/I(50\ ms)$
50 ms	1.00
2 s	1.10
8 s	1.04
32 s	0.87
60 s	0.76
240 s	0.89
900 s	0.94

Figure 6. Results of the ^{31}P static spin echo experiment for the solid solution $GaZn_7PSe[BO_2]_{12}$. (a) The decay in the spin echo intensity as a function of $2\tau_1$; (b) fit of experimental data to Equation 2.

Figure 7. Calculated and experimental values of the second moment for the solution series $Ga_xZn_{(8-x)}P_xSe_{(2-x)}[BO_2]_{12}$. (a) Calculated from Equation 1a assuming phosphorus at all cage centers; (b) calculated from Equation 1a based on the actual number of phosphorus atoms in the sample; (c) c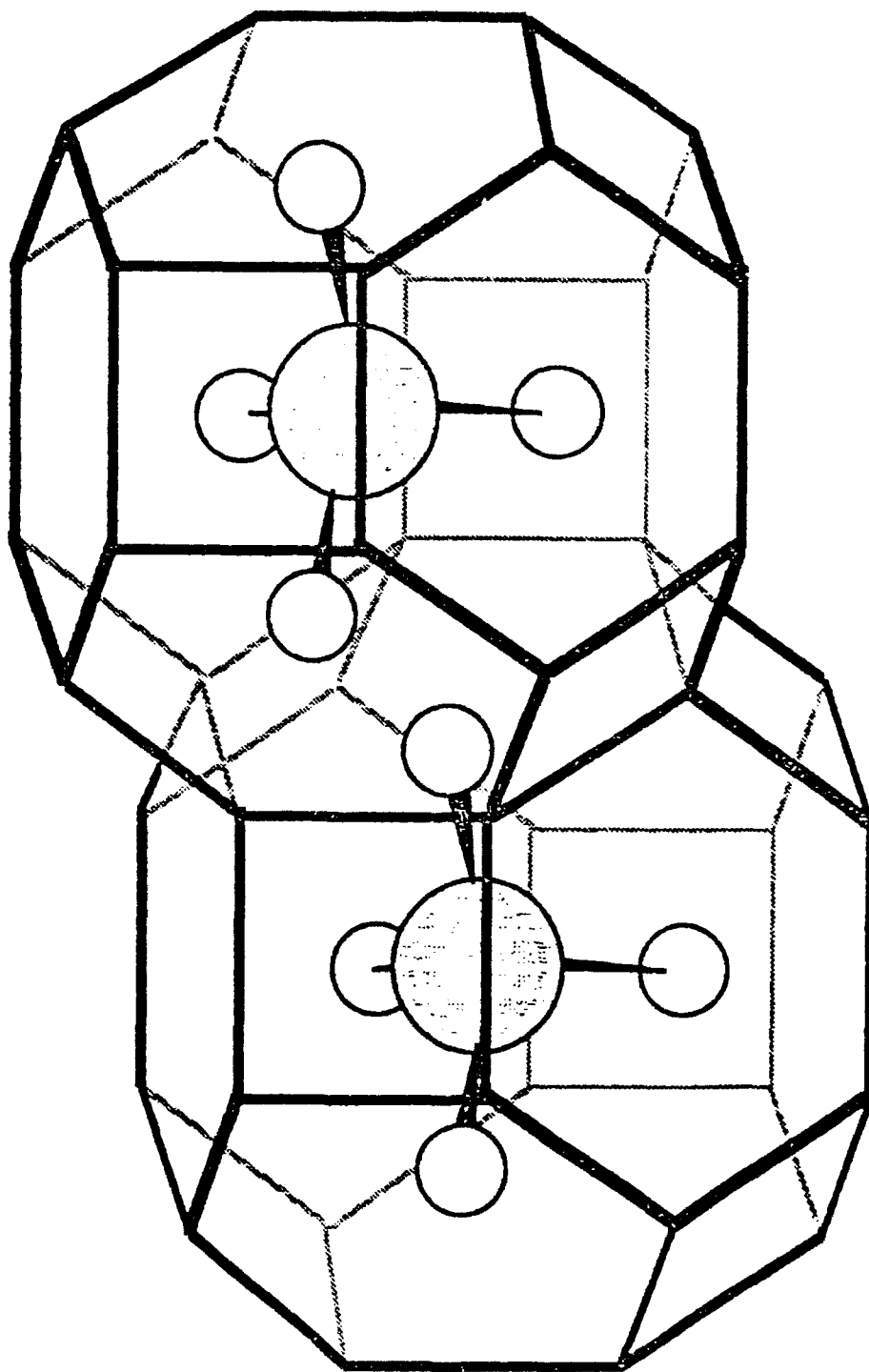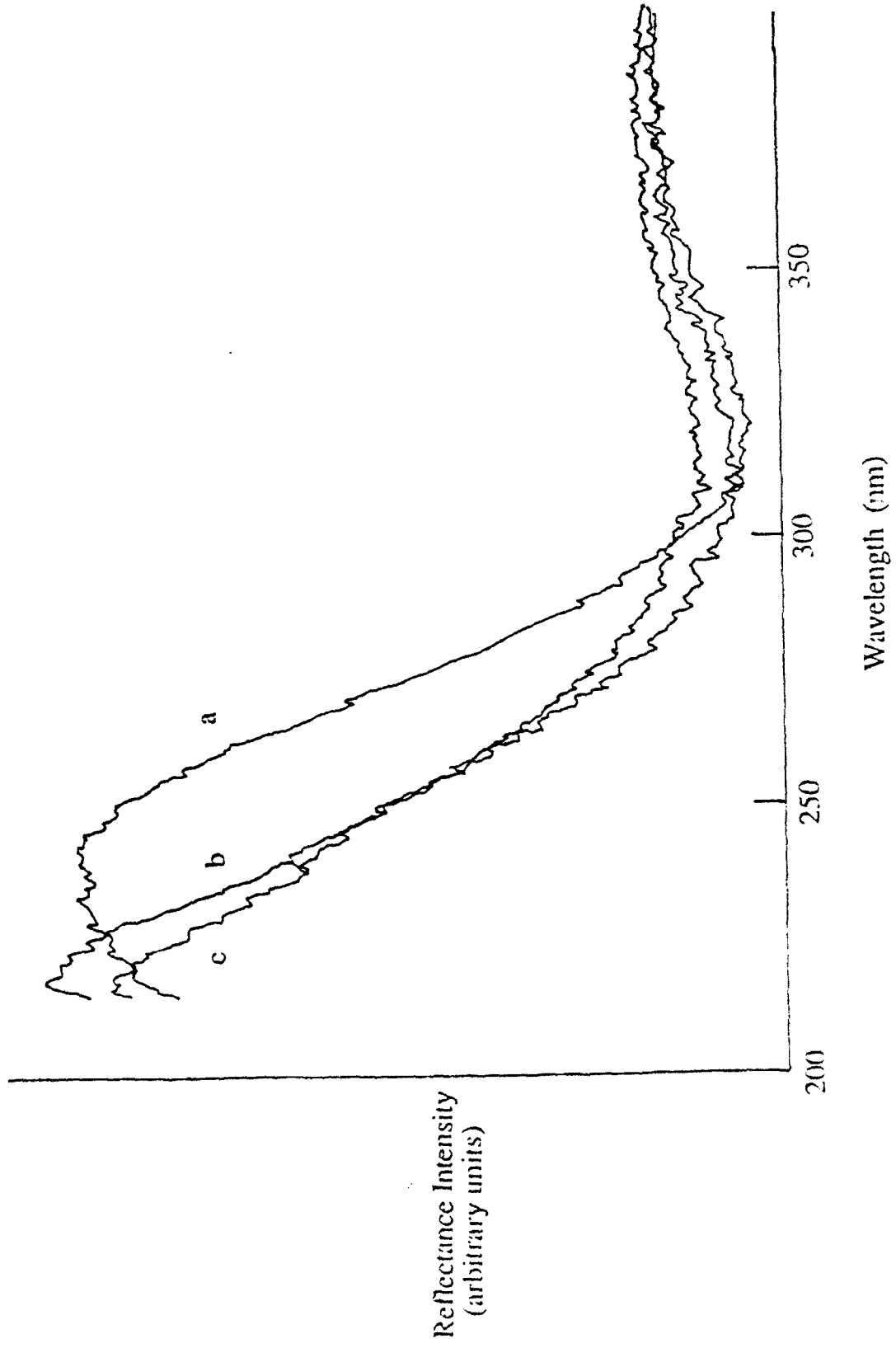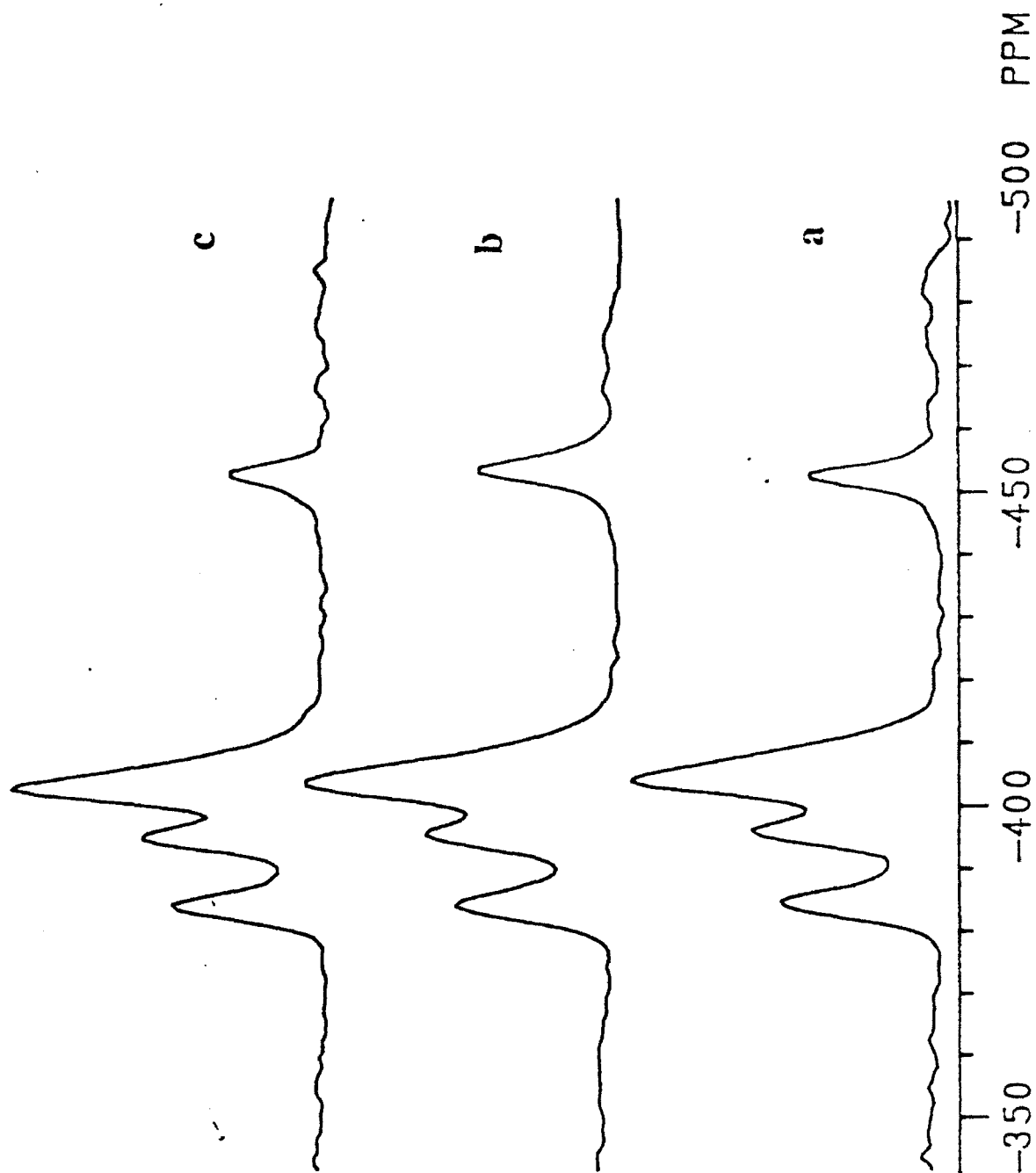alculated from Equation 1b assuming phosphorus at all cage centers; (d) calculated from Equation 1b based on the actual number of phosphorus atoms in the sample.

Fig 1

Fig 2

Fig 3

-500 PPM   -450   -400   -350

c

b

a

Fig 4

To be revised with
theoretical spectra when
they arrive

A B C D

-350   -400   -450   PPM
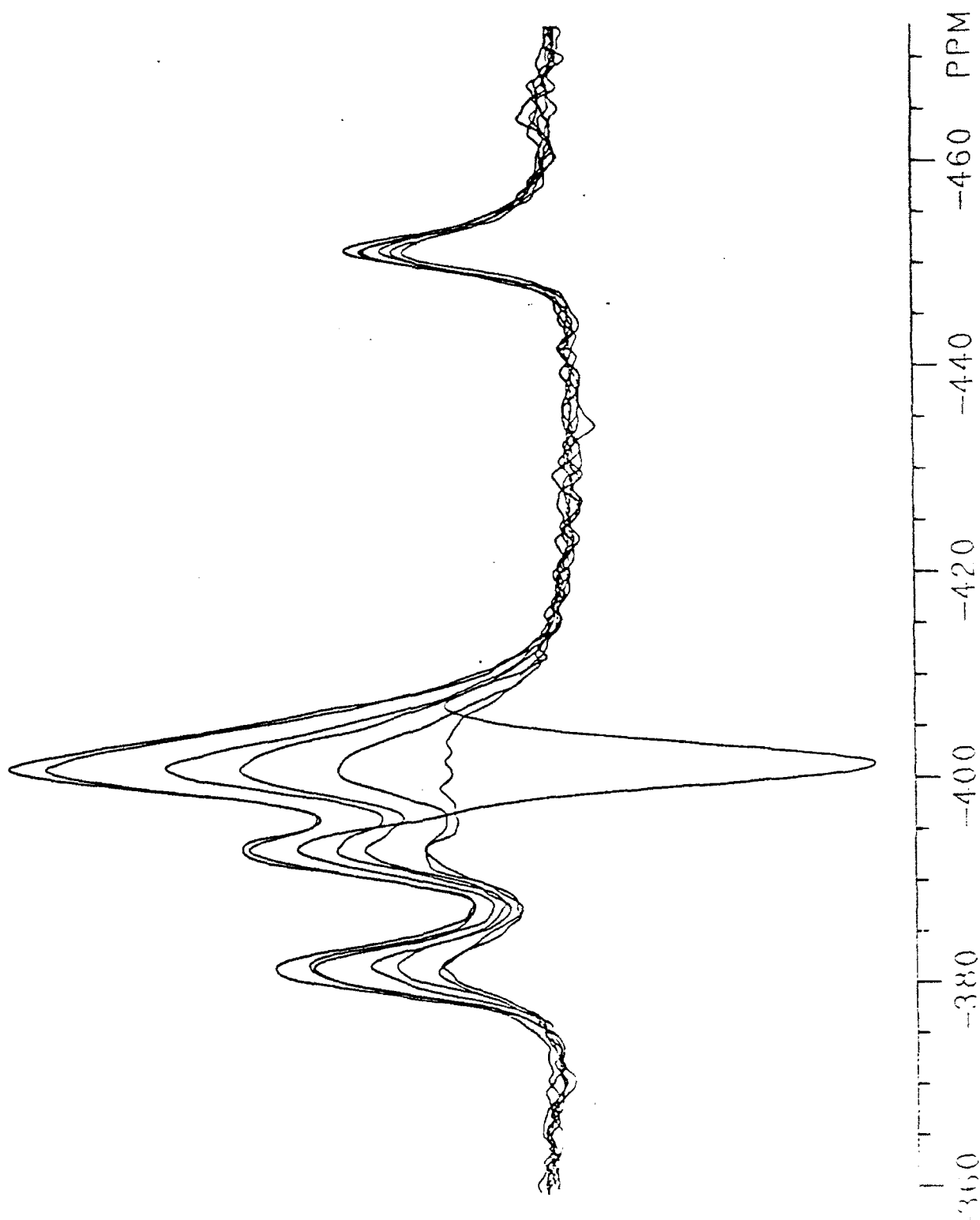
Fig 5

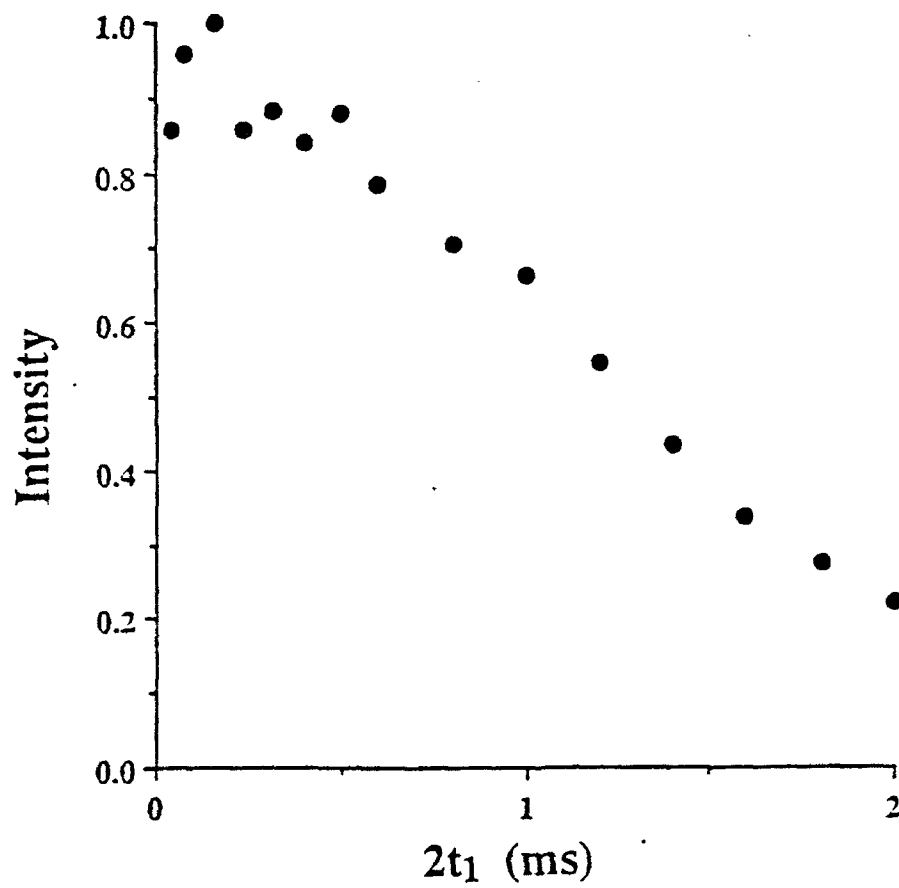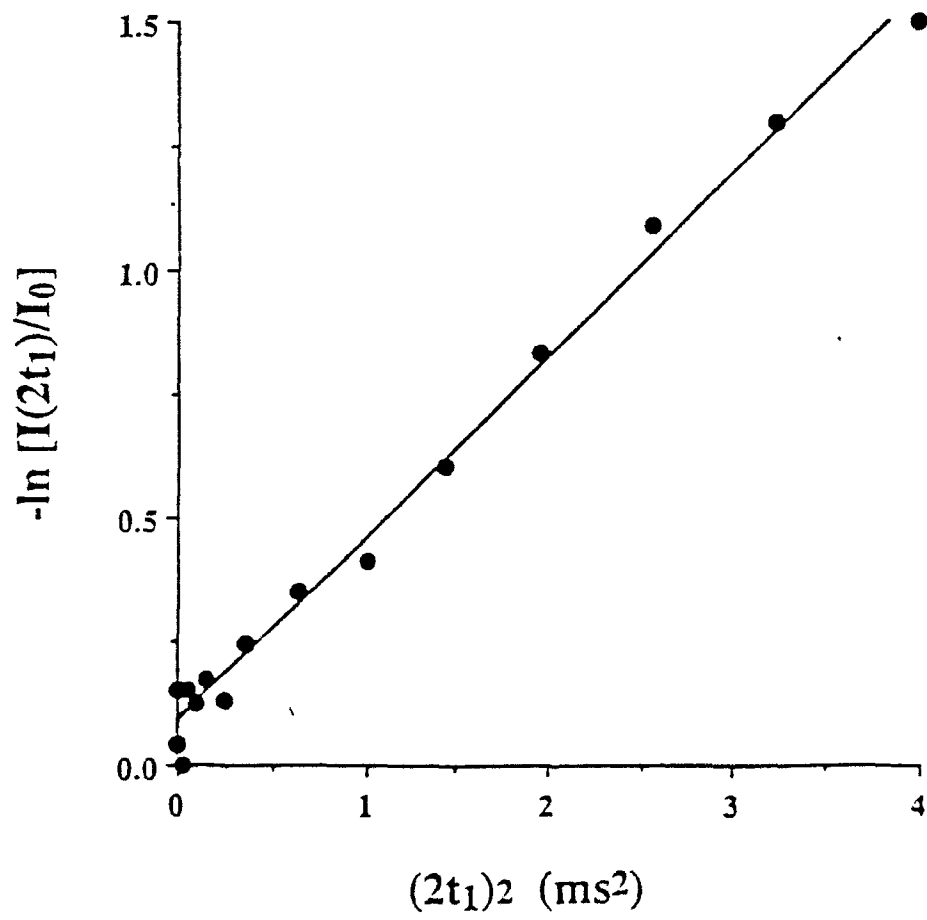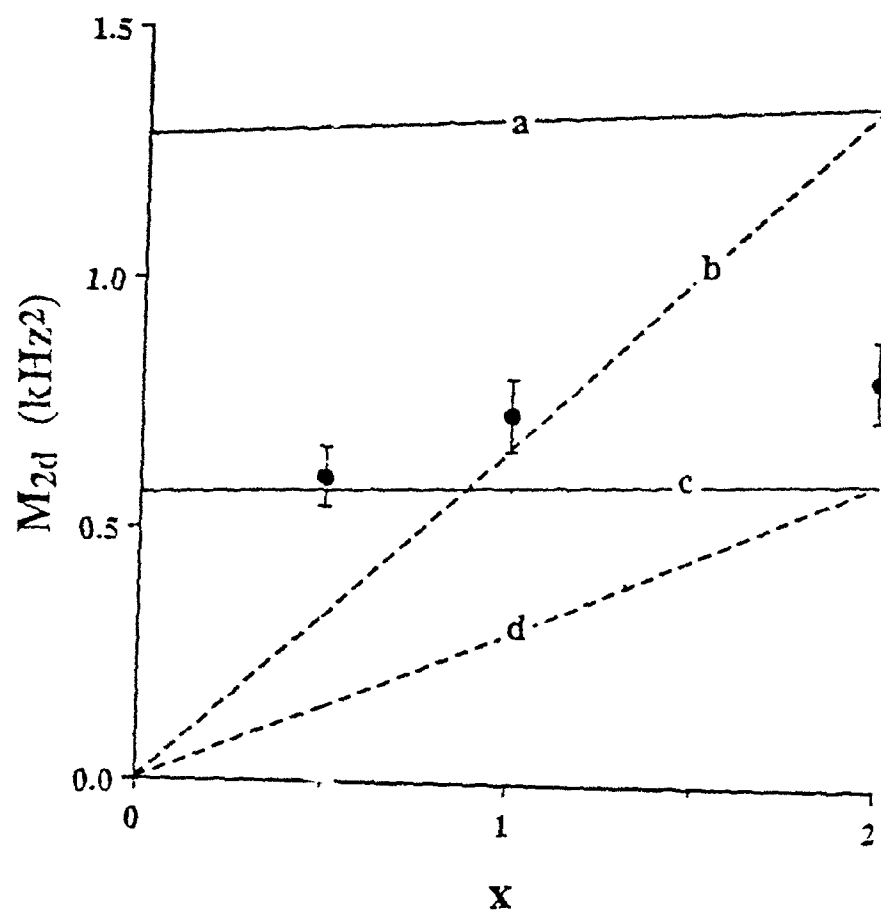-460   -440   -420   -400   -380   -360   PPM
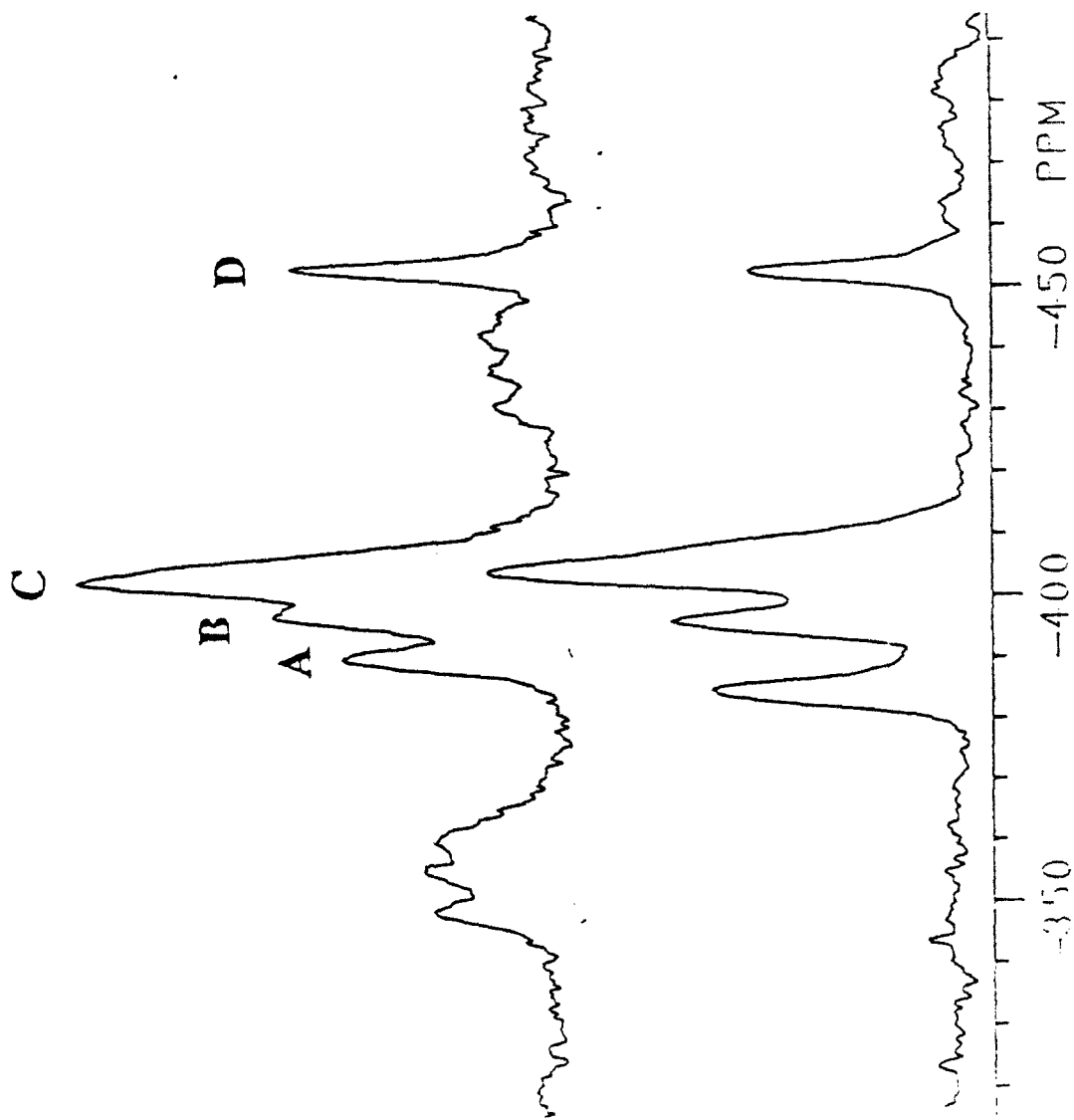
Fig 6b

Fig 7

TECHNICAL REPORT DISTRIBUTION LIST - GENERAL

Office of Naval Research (2)*
Chemistry Division, Code 1113
800 North Quincy Street
Arlington, Virginia 22217-5000

Dr. James S. Murday   (1)
Chemistry Division, Code 6100
Naval Research Laboratory
Washington, D.C. 20375-5000

Dr. Robert Green, Director   (1)
Chemistry Division, Code 385
Naval Air Weapons Center
  Weapons Division
China Lake, CA 93555-6001

Dr. Elek Lindner   (1)
Naval Command, Control and Ocean
  Surveillance Center
RDT&E Division
San Diego, CA. 92152-5000

Dr. Bernard E. Douda (1)
Crane Division
Naval Surface Warfare Center
Crane, Indiana 47522-5000

Dr. Richard W. Drisko   (1)
Naval Civil Engineering
  Laboratory
Code L52
Port Hueneme, CA 93043

Dr. Harold H. Singerman   (1)
Naval Surface Warfare Center
  Carderock Division Detachment
Annapolis, MD 21402-1198

Dr. Eugene C. Fischer   (1)
Code 2840
Naval Surface Warfare Center
  Carderock Division Detachment
Annapolis, MD 21402-1198

Defense Technical Information
  Center   (2)
Building 5, Cameron Station
Alexandria, VA 22314

* Number of copies to forward

12